Ciliary and centrosomal defects associated with mutation and depletion of the Meckel syndrome genes *MKS1* and *MKS3*

Rachaneekorn Tammachote[1,†,‡]**, Cynthia J. Hommerding**[2,†]**, Rachel M. Sinders**[3]**, Caroline A. Miller**[3]**, Peter G. Czarnecki**[4]**, Amanda C. Leightner**[1]**, Jeffrey L. Salisbury**[1]**, Christopher J. Ward**[2]**, Vicente E. Torres**[2]**, Vincent H. Gattone II**[3] **and Peter C. Harris**[1,2,*]

[1]Department of Biochemistry/Molecular Biology, [2]Division of Nephrology and Hypertension, Mayo Clinic, Rochester, MN, USA, [3]Department of Anatomy and Cell Biology, Indiana University School of Medicine, Indianapolis, IN, USA and [4]Department of Medicine, Mayo Clinic, Rochester, MN, USA

Received March 30, 2009; Revised May 22, 2009; Accepted June 5, 2009

Meckel syndrome (MKS) is a lethal disorder characterized by renal cystic dysplasia, encephalocele, polydactyly and biliary dysgenesis. It is highly genetically heterogeneous with nine different genes implicated in this disorder. MKS is thought to be a ciliopathy because of the range of phenotypes and localization of some of the implicated proteins. However, limited data are available about the phenotypes associated with MKS1 and MKS3, and the published ciliary data are conflicting. Analysis of the *wpk* rat model of MKS3 revealed functional defects of the connecting cilium in the eye that resulted in lack of formation of the outer segment, whereas infertile *wpk* males developed spermatids with very short flagella that did not extend beyond the cell body. In *wpk* renal collecting duct cysts, cilia were generally longer than normal, with additional evidence of cells with multiple primary cilia and centrosome over-duplication. Kidney tissue and cells from MKS1 and MKS3 patients showed defects in centrosome and cilia number, including multi-ciliated respiratory-like epithelia, and longer cilia. Stable shRNA knockdown of *Mks1* and *Mks3* in IMCD3 cells induced multi-ciliated and multi-centrosomal phenotypes. These studies demonstrate that MKS1 and MKS3 are ciliopathies, with new cilia-related eye and sperm phenotypes defined. MKS1 and MKS3 functions are required for ciliary structure and function, including a role in regulating length and appropriate number through modulating centrosome duplication.

INTRODUCTION

Meckel syndrome (MKS; also known as Meckel–Gruber syndrome) is a lethal, recessive disorder characterized by renal cystic dysplasia, central nervous system defects (typically occipital encephalocele), polydactyly and biliary dysgenesis. MKS is one of a group of syndromic disorders: nephronophthisis (NPHP), Senior–Loken syndrome (SLS), Joubert syndrome and related disorders (JSRD), Bardet–Biedl syndrome (BBS) and oro-facial-digital syndrome 1 (OFD1) with considerable genic and phenotypic overlap.

The range of phenotypes and emerging data about the implicated proteins indicates that they are associated with ciliary defects; ciliopathies (1). Primary cilia are rooted in the cell through the basal body (a modified centriole), have a sensory role, and are essential for several developmental pathways (2). Nine genes (*MKS1, MKS3, CEP290, RPGRIP1L, CC2D2A, NPHP3, BBS2, BBS4* and *BBS6*) have been associated with MKS or Meckel-like syndrome. Many of these proteins have been localized to the basal body and in some cases the cilium itself (3–7). The specific role of these proteins is not yet known but several have been

*To whom correspondence should be addressed at: Division of Nephrology and Hypertension, Mayo Clinic, 200 First Street SW, Rochester, MN 55905, USA. Tel: +1 5072660541; Fax: +1 5072669315.; Email: harris.peter@mayo.edu
†The authors wish it to be known that, in their opinion, the first two authors should be regarded as joint First Authors.
‡Present address: Department of Botany, Faculty of Science, Chulalongkorn University, Bangkok, Thailand.

implicated in localizing specific proteins to the cilium and to ciliary formation (8).

MKS1 and *MKS3* were the first genes found to be associated with typical MKS and are a common cause of this disorder in non-consanguineous cases (9–11). *MKS3* has also been associated with JSRD (12,13), whereas *MKS1* mutations have been found in BBS; variants in these MKS genes may also influence the disease presentation in BBS (14). *MKS1* encodes a 559 amino acids cytosolic protein that contains a B9 domain (10). MKS1 was localized to the centrosome in renal HEK293 and inner medullary collecting duct (IMCD3) cells and in the *Caenorhabditis elegans* ortholog, XBX-7, was found at the base of the cilium, complexed with two other B9 proteins (15,16). The MKS protein, meckelin, has 995 amino acids and is predicted to be a transmembrane (TM) protein with seven (or three) TM domains with a large extracellular region, including a cysteine rich area, and short cytoplasmic tail (11,17). Meckelin has been localized to cilia in HEK293 and BEC cells, with additional evidence of membrane staining. Previously, cellular depletion of either protein was associated with loss of cilia (15). In genetically undefined MKS livers, some bile ducts were also found to lack cilia, whereas in others they were present (18). The rat model of MKS3, w*pk*, is viable from 3 weeks (Wistar background) (19) to 50 days (Brown Norway background; Gattone, unpublished data) and has rapidly progressive polycystic kidney disease (PKD) and hypoplasia to agenesis of the corpus callosum. In this model, the presence of cilia in kidney epithelia and ventricular ependymal cells has been documented (19). A recently described mouse with a 295 kb deletion including *Mks3* has a similar, viable phenotype with rapidly progressive PKD, hydrocephalus and death by 3 weeks (20).

Here we comprehensively characterize the ciliary phenotype in the *wpk* model and MKS1 and MKS3 kidney and liver tissue and cells. In addition, we document events associated with cellular depletion of these proteins and show evidence of ciliary and centrosomal defects.

RESULTS

Ciliary defects in the *wpk* rat

Due to the lethality of MKS, little is known about the structure of the eye, which is often abnormal in syndromic forms of PKD likely because of defects in the connecting cilium required to form the outer segment (21). Transmission electron microscopy (TEM) analysis of the retina of the *wpk* rat showed failure of development of the outer segment and significant thinning of the outer nuclear layer by 3 weeks, and in older animals (50 days) loss of the rod cells (Fig. 1A and B). Higher resolution analysis showed that connecting cilia were present in *wpk* rats but appeared to be non-functional and disorientated (Fig. 1C).

Analysis of *wpk* rats at 50 days showed that, in contrast to the wild-type where late spermatids had fully formed flagella, no spermatids with long flagella were present (Fig. 2A and B). Staining with acetylated α-tubulin confirmed only a very low level of mature spermatids with flagella (Fig. 2C and D). TEM analysis showed evidence of a small flagellum (that was tubulin positive) that barely extended beyond the cell body (Fig. 2E). This defect probably underlines the apparent infertility of the *wpk* males.

Careful analysis of limb development in the *wpk* rats did not show evidence of post-axial polydactyly (data not shown). Likewise, analysis for *situs inversus* did not indicate laterality problems in the *wpk* rat (data not shown). Liver fibrosis, which is common in MKS, including MKS3 (9), was not detected in *wpk* animals during their 50-day lifespan.

Shortened or lengthened cilia and altered ciliary structures have been found in several murine models of PKD including: the PCK and *Pkhd1^{del2/del2}* models of ARPKD, *Tg737^{orpk}*, *jck* and O*fd1^{+/−}* (22–25). Analysis of *wpk* rats at 50 days by immunofluorescence (IF) and scanning electron microscopy (SEM) showed that although cilia were present on most cells in the cystic collecting ducts, they were more often longer than the wild-type (Fig. 3A–D). In addition, abnormal cells exhibiting centrosome over-duplication were observed at a significantly higher level than in the control (Fig. 3E and F). Cells containing more than one primary cilium were also seen more frequently than in the wild-type, although this did not quite reach significance: $P = 0.07$.

Ciliary and centrosomal defects in MKS1 and MKS3 tissue and cells

Kidney and liver tissue and cells from mutation characterized MKS1 and MKS3 patients were analyzed to provide a fuller view of the effect of mutation on ciliary structure. IF analysis of kidney tissue from a 20-week fetus (R1682) from family M329 with the *MKS3* nonsense mutations R451X and R208X (9) showed considerable variability between cysts, with a significantly higher number of cells with longer cilia than in the control 19-week fetal kidney tissue (Fig. 4A–C and G). In addition, structural abnormalities were detected, including significantly more cells with multiple cilia and multiple centrosomes (Fig. 4D–F). In one cyst, many cells with a multi-ciliated phenotype were detected, reminiscent of cells found in respiratory epithelium with multiple motile cilia (Fig. 4E). Analysis of liver from an 11-week MKS1 case (R1755) from family M383 homozygous for the *MKS1*-Fin$_{major}$ mutation (9) showed that cilia were present in the bile duct (Fig. 4H). Too few bile ducts were available to quantify any ciliary abnormalities.

Molecularly characterized fetal fibroblasts (26 weeks) from patient R1726 (family M376) with the *MKS3* mutations, IVS1-2delA and M252T (9), and placental fibroblasts (20 weeks) from patient R1847 (family M416; unpublished data) homozygous for the *MKS1*-Fin$_{major}$ mutation, were also available for analysis. A 20-week human placental fibroblast cell line was used for comparison. Both the MKS1 and MKS3 cells were found to have a significantly higher level of centrosome over-duplication than the normal control (Fig. 5A and B). The cilia generated from the fibroblasts (normal and MKS) following serum starvation were extremely short and it was not possible to characterize them for defects.

shRNA reduction of *Mks1* and *Mks3* expression results in ciliary and centrosomal duplication

To further test the significance of the observations from *MKS1* and *MKS3* tissue and cells, and the *wpk* rat, we developed an experimental system to deplete these proteins in renal
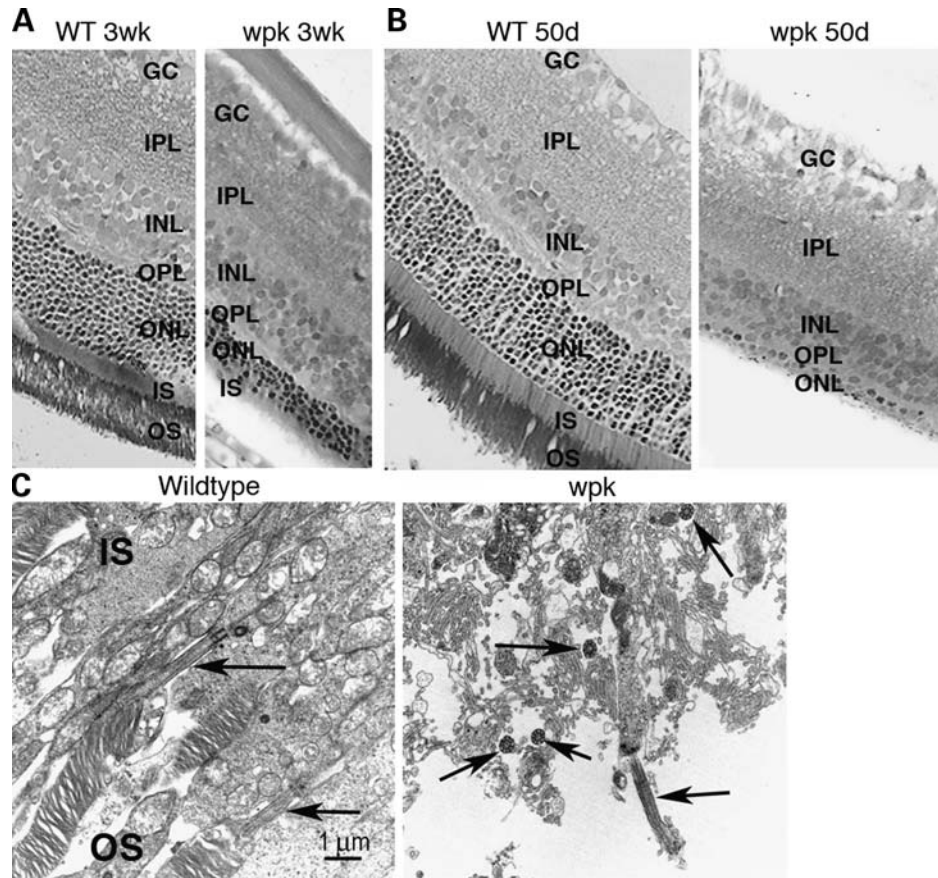
Figure 1. Analysis of the *wpk* eye reveals a retinopathy. (**A**) TEM sections from wild-type (WT) and *wpk* animals show a failure to form the retinal outer segment (OS) at 3 weeks with a significant reduction in the outer nuclear layer (ONL). (**B**) By 50 days in the BN background, the ONL was almost completely absent. (**C**) TEM shows outer and inner segment (IS) formation in wild-type and *wpk* rats at 3 weeks. Although the OS does not form in the *wpk*, connecting cilia (arrows) are present. GC (ganglion cell), IPL (inner plexiform layer), INL (inner nuclear layer) and OPL (outer plexiform layer).
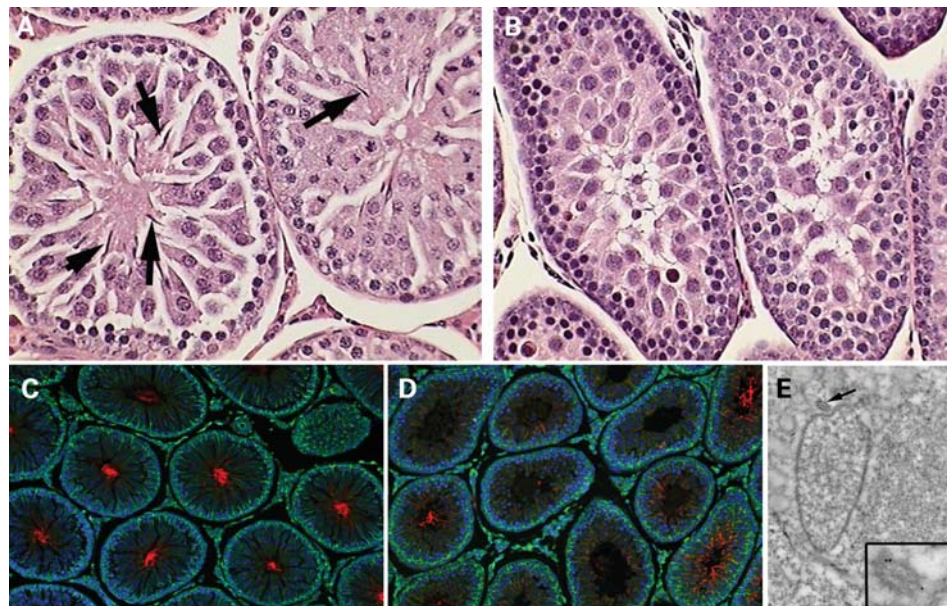

Figure 2. *wpk* sperm have very short flagella. H and E stained sections of wild-type (**A**) and *wpk* (**B**) testis from 50-day BN rats show mature spermatids with long flagella are only found in the wild-type. IF with acetylated α-tubulin (red) and DAPI (blue) shows very few mature spermatids with flagella in *wpk* testis (**D**), compared with wild-type (**C**). (**E**) Immuno-EM analysis of spermatids from *wpk* rats detected with tubulin. Only a small flagella that does not project beyond the cell body, but is tubulin positive (see insert), is detected in the *wpk*.
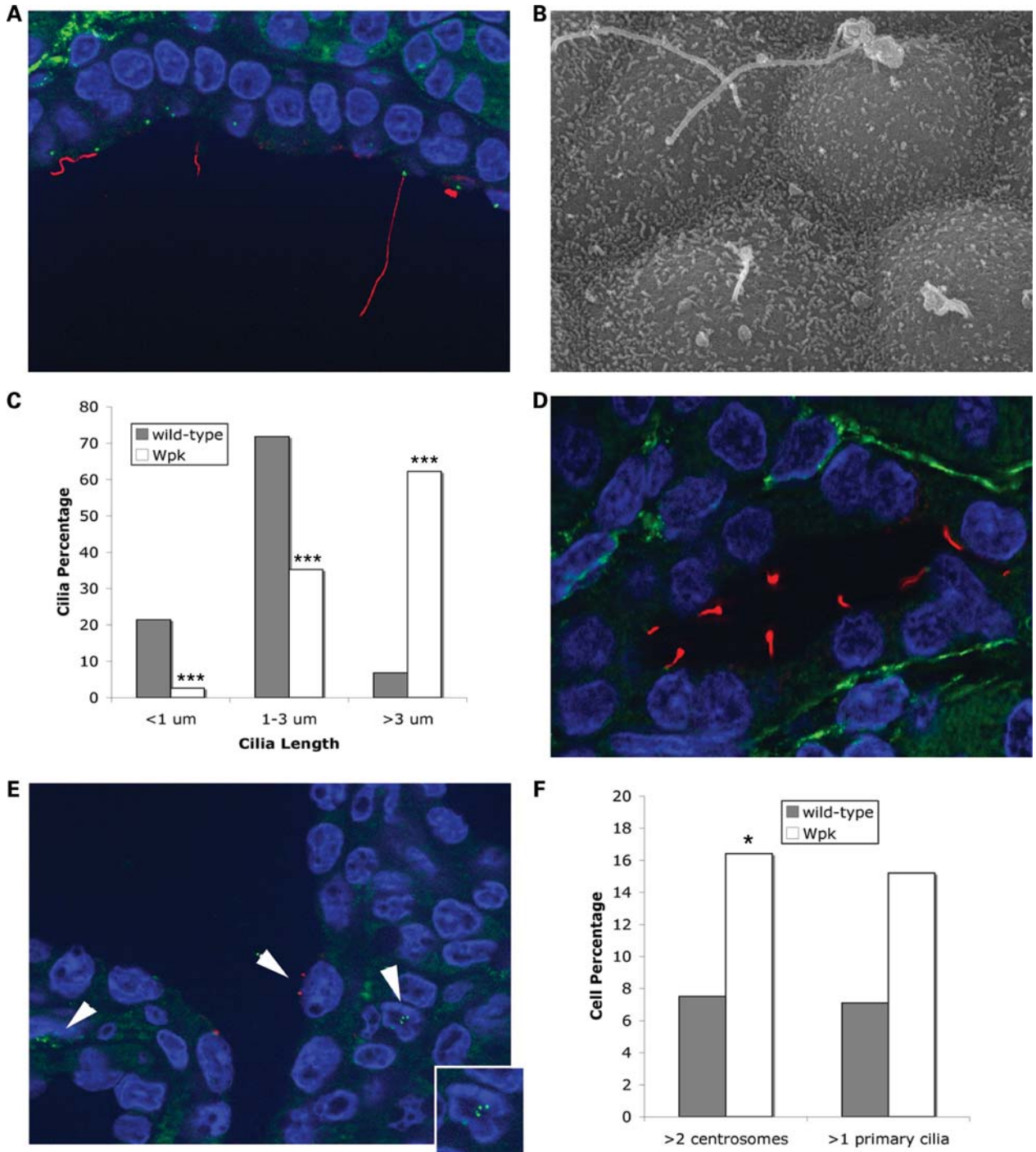
Figure 3. Analysis of cilia length and abnormalities of centrosome and cilia number by IF and SEM in 50-day *wpk*, kidney tissue compared with normal. (**A**) IF with acetylated α-tubulin (red); γ-tubulin (green) and DAPI (blue) and (**B**) SEM of *wpk* cyst linings showing cilia of variable lengths. (**C**) Proportion of cilia <1 μm, 1–3 μm and >3 μm in wild-type (WT; *n* = 103) and *wpk* rats (*n* = 230) in collecting duct cysts; ***P < 0.001. (**D**) Example of IF of wild-type tubule (staining above) showing relatively evenly lengthened cilia. (**E**) Example of IF (as above) showing *wpk* cells with two primary cilia (arrowhead) and multiple centrosomes (arrowheads and insert). (**F**) Quantification of numerical abnormalities. Centrosomes: wild-type (*n* = 120), *wpk* (*n* = 140); *P < 0.05; cilia: wild-type (*n* = 113), *wpk* (*n* = 92); P = 0.07.

epithelial cells. Previous studies employing transient siRNA transfection of IMCD3 cells suggested that depletion resulted in a failure of centriole migration to the apical membrane and reduced cilia formation; cilia were shorter than normal when present (15). To more rigorously test the results of long-term depletion, we established stable IMCD3 cell lines expressing shRNAs that targeted two regions of *Mks1* and three of *Mks3* (see Materials and Methods for details). Specific
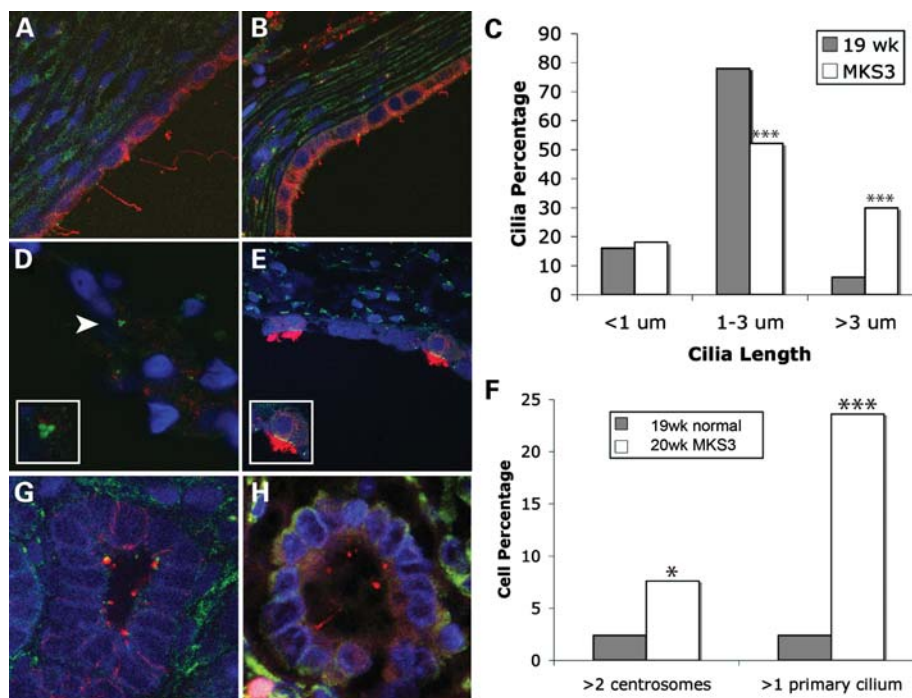
Figure 4. Analysis of ciliary and centrosomal defects in MKS3 (kidney; **A**–**F**), normal kidney (**G**) and MKS1 (liver; **H**) tissue. IF with acetylated α-tubulin (red); γ-tubulin (green) and DAPI (blue) of cyst linings showing long (A) or short cilia (B). (C) Quantification of cilia length: normal (19 weeks; $n = 150$); MKS3 ($n = 144$); ***$P < 0.001$. IF analysis (as above) showing cells with abnormal numbers of centrosomes (D; arrow and inset) and a cyst lining with several multi-ciliated cells (E; close-up in inset). (F) Quantification of cells with abnormal numbers of centrosomes: normal ($n = 169$); MKS3 ($n = 171$); *$P < 0.05$ or cilia: normal ($n = 84$); MKS3 ($n = 148$); ***$P < 0.001$. (G) Normal 20-week kidney showing relatively even cilia lengths. (H) MKS1 biliary duct showing cilia are present.

knockdown clones were selected by Hygromycin B and selection and expression levels of the genes was determined by quantitative real-time PCR (qPCR). Relative expression levels were normalized to the expression of a housekeeping gene (cyclophilin) and compared with those found in untransfected IMCD3 cells (Supplementary Material, Fig. S1).

Cells were grown to incomplete confluence (4 days) for centrosome analysis and 8 days, with at least 2 days at confluence, for analysis of cilia. In both the *Mks1* and *Mks3* cells, protein depletion did not inhibit cilia formation with the proportion of cells with cilia similar to the wild-type control. However, abnormalities in cilia number were seen for *Mks3*, with significantly more cells with multiple cilia than in the wild-type cells detected by IF and scanning EM (Fig. 6A–C). A tendency for more cells with greater than one primary cilium was also seen with *Mks1* depleted cells, but this was not significant (Fig. 7A–C). More dramatic was the proportion of cells that showed centrosome over-duplication with multiple centrosomes seen in up to 16% of *Mks1* depleted cells and 15% of *Mks3* (Figs 6 and 7). As cilia of cultured cells are not under the same constraints to regulate length as those in intact tubules, we did not attempt to monitor the depleted cells for ciliary length defects.

These results are somewhat different from those of Dawe *et al*. (15) where the major phenotype was loss of cilia. A significant difference between the two studies was the knockdown system; transient versus stable. As a result, their assays were performed 96 h after transfection and plating, compared with 8 days after plating and at least 2 days at confluence. Therefore, the apparent lack of cilia (15) may reflect insufficient time after transfection (and reaching confluence), especially if the *Mks* transcripts slowed cellular growth.

DISCUSSION

Comprehensive analysis of the phenotypes in the *wpk* rat, human tissue and cells, and experimental systems has provided a much clearer view of defects associated with *MKS1* and *MKS3* mutation. New cilia-related phenotypes have been identified and structural and numerical ciliary and centrosomal changes characterized, reinforcing the view that MKS is a ciliopathy. However, phenotypic differences between MKS1 and MKS3 and the lack of some characteristic ciliopathy phenotypes show the complexity of this group of disorders and provide clues to function.

A newly identified MKS defect is the lack of outer segment formation in retina of the *wpk* rat. This is somewhat akin to the defect in *Bbs1*$^{M390R/M390R}$, *Bbs2*$^{-/-}$, *Bbs4*$^{-/-}$ and *Bbs6*$^{-/-}$ mice where the outer segment forms but degenerates as the animals age; disease thought to be due to dysfunctional intraflagella transport (IFT) in the connecting cilium (21,26–29). Connecting cilia are present in the *wpk* retina but the inner to outer segment interface is disorganized with no evidence of outer segment formation. It, therefore, seems that the level of ciliary dysfunction may be greater than in BBS and
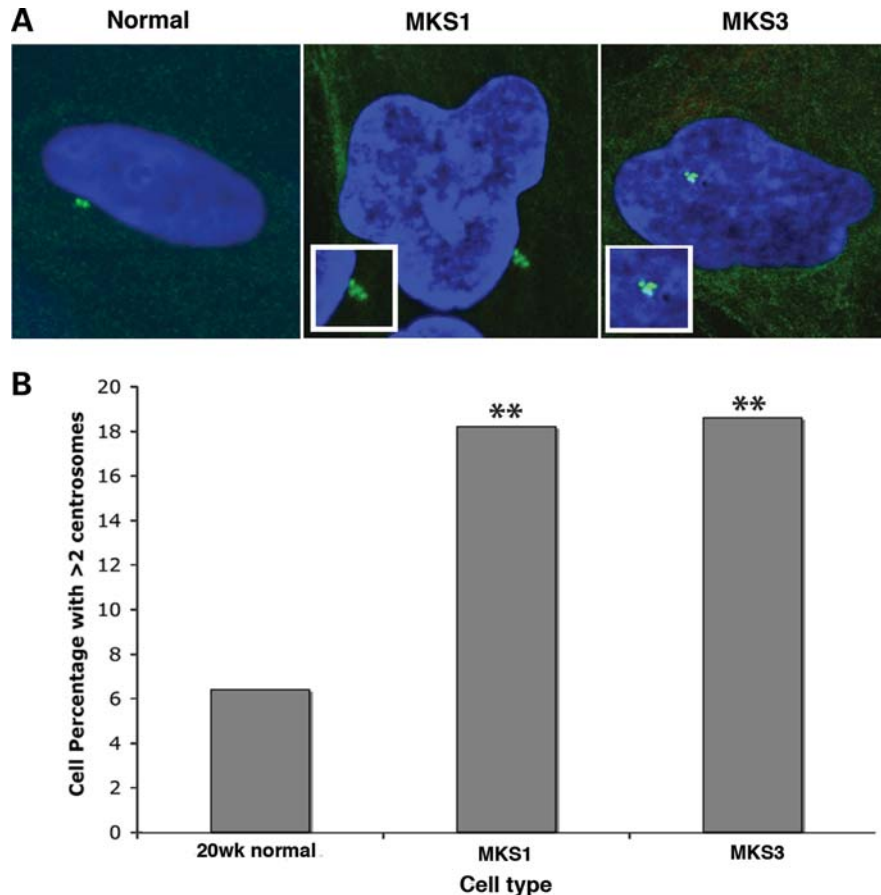
Figure 5. MKS1 and MKS3 fibroblast cells show evidence of multiple centrosomes. (**A**) IF with γ-tubulin (green) and DAPI (blue) shows multiple centrosomes in MKS1 and MKS3 cells (inset). (**B**) Histogram showing cells with more than two centrosomes: normal ($n = 173$); MKS1 ($n = 121$); MKS3 ($n = 102$); **$P < 0.01$.

similar to that in the $Tg737^{orpk}$ model, defective in the IFT protein IFT88 (30). Retinal defects are commonly found in syndromic forms of PKD, including SLS, JSRD and BBS. Owing to the lethality of MKS, little is known about eye defects but MKS associated genes, including *CEP290* and *CC2D2A*, have been associated with the eye diseases, Leber congenital amaurosis and retinitis pigmentosa, respectively (31,32). Recently, hypomorphic *MKS3* mutations were associated with a variant of JSRD (COACH syndrome) with six patients having retinal defects, including coloboma and optic-disc abnormalities (13). Given the *wpk* data, it seems that retinal defects are likely typical in MKS3.

Defects in sperm flagella were evident in the *wpk* that probably explain the infertility of the males even in the BN background where they are viable to 50 days. This defect is similar to that in *Bbs1, 2, 4* and *6* null mice where flagella did not appear to form (26–29). However, detailed TEM analysis of *wpk* sperm showed that short flagella, positive for tubulin, developed but did not elongate beyond the cell body, indicating a defect in appropriate length regulation rather than formation.

Although ciliary defects were found in many organs, lack of *situs inversus* or evidence of digital defects in the *wpk* indicated that nodal and limb bud cilia are not defective in this

model. Polydactyly is only rarely associated with MKS3, and *situs inversus* has not been described in MKS3 (9,17). A recently described mouse model of *Mks3* also did not develop polydactyly or *situs inversus* (20). Therefore, despite the severity of the MKS3 phenotype, it is not associated with universal loss or even functional defects of cilia in every organ, but more subtle structural and function changes in specific locations, which may be associated with expression differences.

Cystic collecting duct epithelia in the *wpk* and MKS3 patients displayed longer cilia. One theory of how defective cilia result in cyst formation is related to mechano-detection of flow. The autosomal dominant PKD (ADPKD) proteins, PKD1 and PKD2 (polycystin-1 and -2), are thought to complex on cilia and form a flow-detector with a Ca^{2+} influx through the polycystin-2 channel important for maintaining intracellular Ca^{2+} homeostasis and epithelial cell differentiation (33). Cilia length has been described as normal in $Pkd1^{-/-}$ cells, or as slightly shorter in human PKD1 cystic epithelia (33,34). Cilia in the *inv* model (NPHP2) appeared normal in terms of length and ability to detect flow (35). However, mice inactivated for the KIF3A subunit of the IFT kinesin-II motor in the collecting duct developed cysts that lacked primary cilia; as did renal cysts
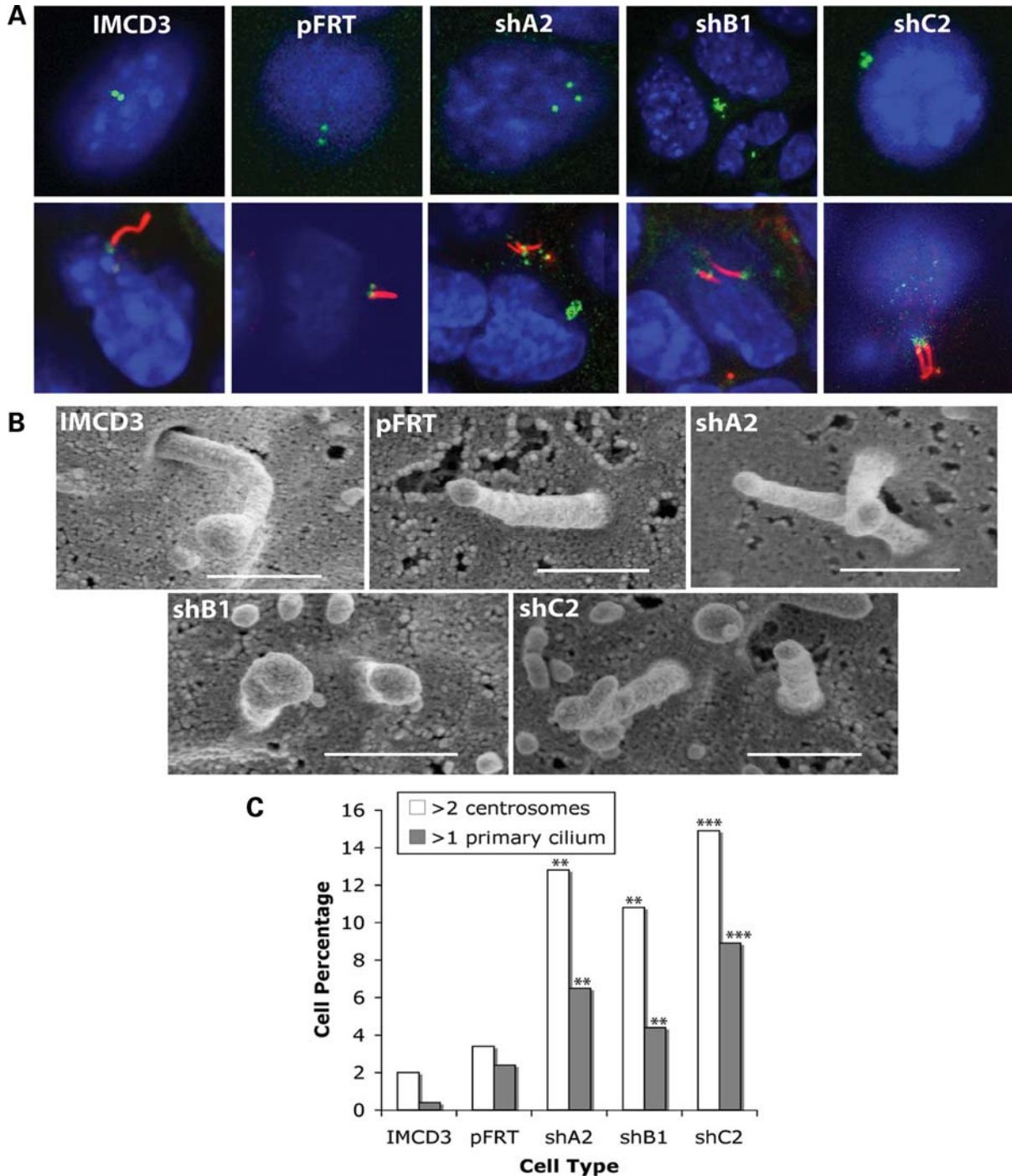
Figure 6. Analysis of centrosomal and ciliary changes associated with shRNA depletion of *Mks3*. (**A**) IF with acetylated α-tubulin (red); γ-tubulin (green) and DAPI (blue), and (**B**) SEM (scale bar 500 nm) shows examples of centrosome over-duplication and more than one cilium per cell in the shA2, shB1 and shC2 knockdown clones, compared with wild-type (IMCD3) and empty vector control (pFRT). (**C**) Quantification of centrosome over-duplication: IMCD3 ($n = 198$); pFRT ($n = 119$); shA2 ($n = 94$); shB1 ($n = 151$); shC2 ($n = 161$); $^{**}P < 0.01$; $^{***}P < 0.001$; and numerical ciliary defects: IMCD3 ($n = 241$); pFRT ($n = 84$); shA2 ($n = 107$); shB1 ($n = 159$); shC2 ($n = 157$); $^{**}P < 0.01$; $^{***}P < 0.001$.

in *Ofd1*$^{+/-}$ females (22,36). The more typical finding, nonetheless, from models of PKD is a quantitative change. This manifested as: shorter cilia in biliary epithelia of *Pkhd1* mutants (24,25) and the *Tg737*^{orpk} model (37); longer cilia in the *jck* (23), *Nphp3*$^{-/pcy}$ (38) and *Mks3* mouse models

(20); and cilia more variable in length in the *cpk* model (39). It appears that meckelin, in common with other syndromic PKD proteins, plays a role in regulating the length of the cilia/flagella. The polycystin flow complex may, therefore, function poorly on cilia of inappropriate length and cyst
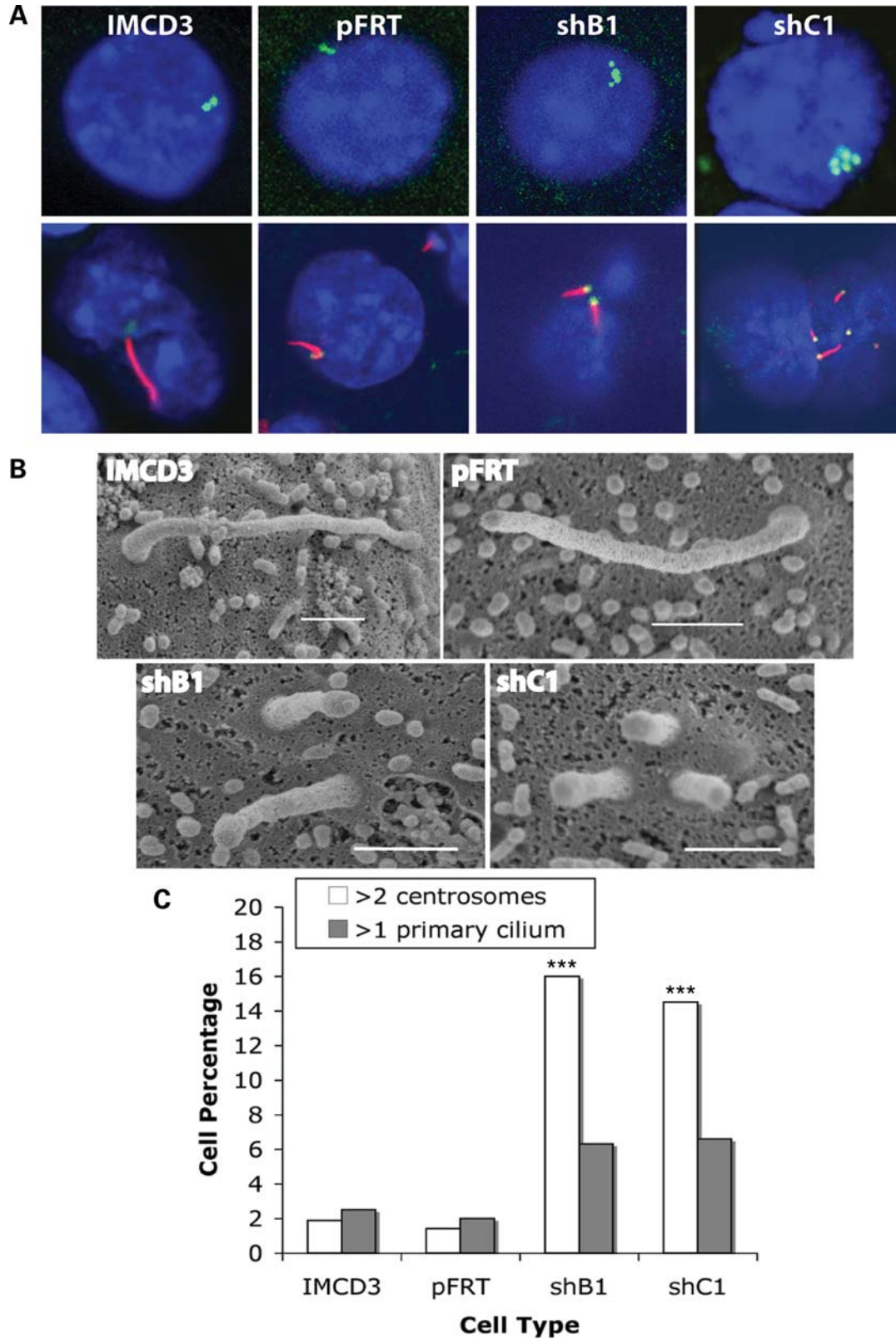
Figure 7. Analysis of centrosomal and ciliary changes associated with shRNA depletion of *Mks1*. (**A**) IF with acetylated α-tubulin (red); γ-tubulin (green) and DAPI (blue), and (**B**) SEM (scale bar 500 nm) shows examples of centrosome over-duplication and more than one cilium per cell in the shB1 and shC1 knock-down clones, compared with wild-type (IMCD3) and empty vector control (pFRT). (**C**) Quantification of centrosome over-duplication: IMCD3 ($n = 159$); pFRT ($n = 148$); shB1 ($n = 162$); shC1 ($n = 152$); ***$P < 0.001$; and numerical ciliary defects: IMCD3 ($n = 199$); pFRT ($n = 199$); shB1 ($n = 127$; $P = 0.14$); shC1 ($n = 122$; $P = 0.09$).

development result. However, it seems likely that the length defects may be symptomatic of wider problems with cargo transport in the cilium, and inappropriate positioning of protein cargos leading to cyst development; highlighting possible roles for the MKS proteins.

Studies in Chlamydomonas have identified mutants defective in regulating flagella length that result in longer or shorter flagella (40,41). It has been suggested that length mutants play a role in regulating IFT and that a balance between flagella assembly and disassembly determines length (42,43). Flagella in Chlamydomonas length mutants often also display structural abnormalities with bulbous ends containing IFT proteins (40,41). Similar defective ciliary structures have been found in many ciliopathies, including *Tg737^{orpk}* (44), murine models of ARPKD (24,25) and *Bbs1* and *Bbs2* null mutants (35,37). As well as bulbous ends, these abnormal structures included branched and 'star burst' cilia.

In *wpk* tissue, MKS1 and MKS3 cells and tissue and depleted cells, as well as length problems, ciliary defects manifested as cells with more than one cilium and over-duplicated centrosomes; extreme examples of multi-ciliated cells were seen in MKS3 tissue. Multiple cilia have been found in 12.8% of *orpk^{-/-}* kidney cysts at P14 (45). Precise regulation of centrosome duplication to once per cell-cycle during mitosis is required to prevent the formation of multipolar spindles and genomic instability. Centrosome over-duplication is commonly found in cancer and has been proposed to be an early defect that underlies much of the aneuploidy seen in solid tumors (46–48). Recently, depletion of polycystin-1 was associated with centrosome amplification in cellular systems with similar phenotypes found in *Pkd1^{-/-}* cells and ADPKD cystic tissue (49). Centrosome amplification in the cellular systems resulted in mitotic catastrophe, but ultimately stabilized clones with less extreme aneuploidy predominated. Karyotypic changes have been detected in ADPKD cyst lining cells (50). Cell lines derived from a PKD2 transgenic mouse were also found to have centrosome amplification and genomic instability (51). Interestingly, cells overexpressing *MKS3* often formed multinucleated cells (15), possibly related to centrosome amplification. It is not clear to what extent genomic instability and resulting aneuploidy are associated with cyst development in MKS because both human MKS1 and MKS3 and *wpk* cyst development are extremely rapid resulting in enlarged and cystic kidneys by 20 weeks gestation or by 20d post-partum, respectively. However, our data indicate that MKS joins an increasing list of forms of PKD where numerical as well as length defects to cilia are associated with cyst development.

In MKS3 mutant kidney tissue, we identified multi-ciliated cells that are not normally found in the mammalian kidney. Occasional reports of cells with multiple motile cilia have been described in patients with hypercalcemia or nephrotic syndrome (52–56). In zebrafish, the pronephric duct has a mixture of cells with multiple motile cilia that generate flow and those with just one primary cilium: jagged 2/Notch signaling modulates the number of multi-ciliated cells (57,58). Over-expression of proteins involved in regulating centriole duplication, such as Plk4 or Sas-6, can result in centriole reduplication and *de novo* assembly of centrioles in acentriolar

cells (59,60). Our data indicate a role for MKS1 and meckelin in regulating the process of centrosome duplication relative to the cell-cycle and even the formation of multi-ciliated cells. The cellular system we have developed may help to understand this process.

The process of planar cell polarity (PCP), a non-canonical branch of the Wnt signaling pathway, has been implicated in MKS because of the exencephaly and PKD phenotypes (61,62). The centrosomal NPHP2 protein, inversin, is thought to act as a molecular switch between the canonical and non-canonical Wnt signaling pathways (63), and PCP has been implicated in the process of ciliogenesis (64). Preliminary data highlighted possible defects in the PCP process of convergent extension in *mks1* depleted zebrafish; *MKS1* variants may also enhance the phenotype associated with *BBS* mutations (14). Loss of many core PCP proteins is associated with craniorachischisis, an open neural tube defect similar to an encephalocele (65); *Bbs4* null animals also occasionally develop exencephaly (21). Lengthening of tubules in the kidney requires coordinated cell division with the orientation of the mitotic spindle along the axis of the tubule, a process modulated by PCP (61). Significant spindle misorientation was noted in the PCK and *Hnf1β* models of PKD, potentially resulting in tubule dilatation. Our data indicate defects in the regulation of centrioles and, given their role as mitotic spindle poles, questions whether this is directly related to the cystic expansion and exencephaly through interaction of MKS1 and meckelin in the PCP pathway. An alternative explanation is that the defects found in MKS reflect problems with appropriate ciliogenesis and, therefore, disrupts the multiple pathways that require functional cilia to operate. The *wpk* rat and MKS cellular systems are likely to be central to understand which mechanism predominates.

MATERIALS AND METHODS

Wpk rats

Animals were housed at the Indiana University School of Medicine, Laboratory Animal Resource Center, and maintained as previously described (19). The *wpk* rat was maintained in both the Wistar and Brown Norway (BN) backgrounds. Animals were genotyped using a Taqman assay with fluorescent probes for the mutant single nucleotide change and wild-type (details available on request). The renal phenotype was evaluated in 50-day *wpk* BN rats and wild-type controls. The eye phenotype was evaluated in *wpk* rats in both backgrounds at 3 weeks and 50 days. The sperm phenotype was evaluated in 50-day *wpk* BN males.

Transmission electron microscopy

wpk rats were perfused through the left ventricle with 4% paraformaldehyde in 0.1 M phosphate buffer. Tissue sections used for electron microscopy were placed in 2% paraformaldehyde, 2% glutaraldehyde. Tissue was processed for TEM by the EM core at the Indiana School of Medicine, Indianapolis using standard methods. Briefly, tissue segments were cut into 1 × 2 mm segments, post-fixed in osmium tetroxide, dehydrated in a graded series of ethanol, infiltrated and embedded in

Embed 812 (Electron Microscopy Sciences). Sections were cut with a diamond knife on a Leica UCT Ultramicrotome (Leica), stained with lead citrate/uranyl acetate and viewed on a Tecnai G2 12 Bio Twin (FEI). Immunogold labeling of testis tissue was performed post-embedding, on sections prepared for TEM. Anti-acetylated α-tubulin (Sigma, T6793) was used to label sperm flagella, and gold conjugated anti-mouse secondary (Amersham, #RPN424) was used.

Hematoxylin and eosin staining

wpk rats, at 50 days, were perfused as above and testis processed for paraffin embedment, and sections stained with hematoxylin and eosin.

Human tissue

Tissue and cells from MKS3, MKS1 and normal fetuses was collected following termination as approved by the relevant Institutional Review Board and after obtaining parental consent. Fibroblast cell lines established from fetal or placental patient material and a normal placental fibroblast cell line (ATCC, CRL-7548) were also employed. Fibroblasts were cultured in Advanced D-MEM/F-12 (Invitrogen) supplemented with 5% fetal calf serum, glutamine and penicillin/streptomycin (Gibco). Prior to analyses, cells were grown for up to 4 days for centrosome studies (less than 80% confluent), and serum starvation was carried out by decreasing the serum concentration from 5 to 0.2% for up to 8 days to induce ciliation. Tissue for IF was formalin fixed, or for fibroblasts methanol fixed, and stained as indicated below.

Generation of *Mks1* and *Mks3* shRNA constructs

The mouse *Mks1* and *Mks3* gene sequence was analyzed for potential shRNA targets based on the predicted secondary structure of the mRNA transcript of interest. Energetically favorable stems were predicted from the input sequence by the Genebee program (http://www.genebee.msu.su/services/rna2_reduced.html). Two targets were successfully developed for *Mks1* (B = TCGGAAGACTTCATCAAGAAC, C = GGACCTGGGACCCTATGGA) and three for *Mks3* (A = GAGCATATGGAGAACGTATTTC, B = CTGCGACTT-CAACCAGTAC, C = GGCCATATATTAGTGGAAAG). Each of the sequences was modified to contain a *Bam*HI site (GGATCC), a *Hin*dIII site (AAGCTT) and 5′ phosphate group. The complementary single-stranded oligonucleotides were annealed and inserted into the pFRT-H1p vector for stable transfection and selected with hygromycin-containing media.

Total RNA extraction, reverse transcription and qPCR

Total RNA was extracted from cultured cells with the RNAeasy kit (Qiagen). Five micrograms of total RNA was reverse transcribed with Random Primers and SuperScript III Reverse Transcriptase (Invitrogen) according to the manufacturer's instruction.

Real-time PCR was used to measure the decrease of the *Mks3* or *Mks1* transcript level following shRNA treatment.

qPCR was employed using SYBR Green ER universal supermix (Invitrogen, 11762-100) according to manufacturer's instruction on an Opticon DNA engine (BioRad). The expression of these transcripts was compared with a housekeeping control gene (Cyclophilin: forward primer 5′-CCCACCGTGTTCTTCGACATCACG-3′, reverse primer 5′-GCTGTCTTTGGAACTTTGTCTGCA-3′). All primers were designed by GeneScript (https://www.genscript.com/ssl-bin/app/primer) and were specifically designed to amplify across an intron/exon boundary (*Mks1* forward primer = 5′-GGAGGTTCTTCATTGGCG-3′, reverse primer = 5′-TTGTCTCAGTGCGGAATCC-3′; *Mks3* forward primer = 5′-CAGACACTGAGAGAAGGCTGGAT-3′, reverse primer = 5′-ACAGGGCTGCTGAAGTCAACC-3′).

IMCD3 cell culture and transfection

Mouse IMCD3 cells were cultured under the same conditions as described above for fibroblast culture. For stable transfection of IMCD3 cells, they were grown to ∼80% confluence and transfected with 5 μg of plasmid DNA/1×10^6 cells using Amaxa Cell Line Nucleofector (Solution V, program O17). Cells were selected for stable transfection with 200 μg/ml Hygromycin B (pFRT-H1p), for more than 15 days prior to clone selection for all subsequent assays.

IF microscopy

Antibodies. The monoclonal antibodies T6793 and T6667 (Sigma) to acetylated α-tubulin and γ-tubulin were employed to stain cilia and centrosomes, respectively.

Tissue. Formalin or 4% paraformaldehyde fixed, paraffin-embedded tissue was sectioned at a thickness of 4–6 μm. The sections were placed on charged slides, and baked at 55°C overnight. The slides were deparaffinized in Histoclear (HS-200 National Diagnostics) for 10 min, and then rehydrated in a series of ethanols: 100% (×2), 90, 80, 70 and 50% for 3 min each, followed by a wash in PBS. Antigen retrieval was performed by placing slides in 10 mM sodium tricitrate, and placing the solution in a steamer for 40 min. The slides were allowed to cool and washed for 10 min in 0.1 M glycine. The slides were washed in PBS twice and treated with sodium borohydride (45 288-2; Sigma) in ice-cold Hanks buffered saline (Invitrogen) for 40 min on ice and washed twice in PBS. A hydrophobic barrier was applied to the slides using a DAKO pen (S2002; DakoCytomation). The sections were then blocked with 1% BSA, 0.1% Tween-20 for 30 min and washed once in PBS. Primary antibodies were applied and incubated at various concentrations in 0.5% BSA in PBS for 1 h before washing in PBS three times for 10 min each. Slides were incubated in secondary antibodies diluted in 0.5% BSA for 30 min and washed in PBS three times for 10 min each. Prior to the last wash, specimens were incubated in DAPI at 1 μg/ml in PBS for 1 min and washed once in PBS. Sections were mounted with Vectashield (H-100, Vector Laboratories).

Cultured cells. Cells were fixed in either ice-cold methanol or 4% paraformaldehyde in PBS for 5 min, quenched in 100 mM NH_4Cl for 5 min, then blocked with 1% BSA,

5% goat serum, 0.5% Triton X-100 in PBS for 45 min. Cells were incubated in primary antibodies (diluted 1:500 in 1% BSA in PBS) for 1 h, washed three times with PBS, 5 min each and incubated with Alexa Fluor-conjugated secondary antibodies (Molecular Probes) for 1 h. Cell nuclei were counterstained with DAPI, 1:1500 in PBS, and rinsed in PBS before mounting with Vectashield (Vector Laboratories).

Scanning electron microscopy

Cells were grown on glass coverslips for 6–8 days (confluent for at least 2 days), media removed, washed twice in PBS and fixed in Trump's fixative (4% paraformaldehyde, 1% glutaraldehyde). The remainder of the processing was carried out, using standard methods by the EM core facility at Mayo Clinic, Rochester or the EM core at the Indiana School of Medicine, Indianapolis. Briefly, samples were post-fixed in osmium tetroxide, dehydrated in a graded series of ethanol, critical point dried, mounted on stubs and sputter coated with Au/Pd prior to viewing on a JEOL 6390 SEM (JEOL USA Inc.).

Morphometric analysis

Cilia length analyses were performed on both rat and human fixed tissues. The cilia lengths in the rat tissue were measured by SEM on a JEOL 6390 (JEOL USA Inc.) comparing wild-type and *wpk* renal tissues. In the human tissue, cilia lengths were measured by IF staining of paraffin embedded renal tissue sections. Sections were stained with acetylated α-tubulin, γ-tubulin, and nuclei were counterstained with DAPI. Slides were visualized using a Zeiss AxioObserver (Carl Zeiss) microscope at a magnification of ×100. Cilia lengths were then measured using the AxioVision 4.7 software (Carl Zeiss). Mutant cell characterization also employed IF staining with acetylated α-tubulin, γ-tubulin, and nuclei counterstained with DAPI, in all tissues and cells. For all analyses, more than 100 cells were counted for each experimental group.

Statistical analysis

Analysis of the phenotypic characterization data was performed using the Fisher's exact test using Quick Calcs (http://www.graphical.com/quickcalcs/index.ctm). *P*-values were calculated using two tails comparing normal to mutant cell number.

SUPPLEMENTARY MATERIAL

Supplementary Material is available at *HMG* online.

ACKNOWLEDGEMENTS

Conflict of Interest statement. None declared.

FUNDING

REFERENCES

1. Harris, P.C. and Torres, V.E. (2009) Polycystic kidney disease. *Annu. Rev. Med.*, **60**, 321–337.
2. Fliegauf, M., Benzing, T. and Omran, H. (2007) When cilia go bad: cilia defects and ciliopathies. *Nat. Rev.*, **8**, 880–893.
3. Delous, M., Baala, L., Salomon, R., Laclef, C., Vierkotten, J., Tory, K., Golzio, C., Lacoste, T., Besse, L., Ozilou, C. *et al.* (2007) The ciliary gene *RPGRIP1L* is mutated in cerebello-oculo-renal syndrome (Joubert syndrome type B) and Meckel syndrome. *Nat. Genet.*, **39**, 875–881.
4. Gorden, N.T., Arts, H.H., Parisi, M.A., Coene, K.L., Letteboer, S.J., van Beersum, S.E., Mans, D.A., Hikida, A., Eckert, M., Knutzen, D. *et al.* (2008) *CC2D2A* is mutated in Joubert syndrome and interacts with the ciliopathy-associated basal body protein CEP290. *Am. J. Hum. Genet.*, **83**, 559–571.
5. Nachury, M.V., Loktev, A.V., Zhang, Q., Westlake, C.J., Peranen, J., Merdes, A., Slusarski, D.C., Scheller, R.H., Bazan, J.F., Sheffield, V.C. *et al.* (2007) A core complex of BBS proteins cooperates with the GTPase Rab8 to promote ciliary membrane biogenesis. *Cell*, **129**, 1201–1213.
6. Sayer, J.A., Otto, E.A., O'Toole, J.F., Nurnberg, G., Kennedy, M.A., Becker, C., Hennies, H.C., Helou, J., Attanasio, M., Fausett, B.V. *et al.* (2006) The centrosomal protein nephrocystin-6 is mutated in Joubert syndrome and activates transcription factor ATF4. *Nat. Genet.*, **38**, 674–681.
7. Valente, E.M., Silhavy, J.L., Brancati, F., Barrano, G., Krishnaswami, S.R., Castori, M., Lancaster, M.A., Boltshauser, E., Boccone, L., Al-Gazali, L. *et al.* (2006) Mutations in *CEP290*, which encodes a centrosomal protein, cause pleiotropic forms of Joubert syndrome. *Nat. Genet.*, **38**, 623–625.
8. Tallila, J., Jakkula, E., Peltonen, L., Salonen, R. and Kestila, M. (2008) Identification of CC2D2A as a Meckel syndrome gene adds an important piece to the ciliopathy puzzle. *Am. J. Hum. Genet.*, **82**, 1361–1367.
9. Consugar, M.B., Kubly, V.J., Lager, D.J., Hommerding, C.J., Wong, W.C., Bakker, E., Gattone, V.H. II, Torres, V.E., Breuning, M.H. and Harris, P.C. (2007) Molecular diagnostics of Meckel–Gruber syndrome highlights phenotypic differences between MKS1 and MKS3. *Hum. Genet.*, **121**, 591–599.
10. Kyttala, M., Tallila, J., Salonen, R., Kopra, O., Kohlschmidt, N., Paavola-Sakki, P., Peltonen, L. and Kestila, M. (2006) *MKS1*, encoding a component of the flagellar apparatus basal body proteome, is mutated in Meckel syndrome. *Nat. Genet.*, **38**, 155–157.
11. Smith, U.M., Consugar, M., Tee, L.J., McKee, B.M., Maina, E.N., Whelan, S., Morgan, N.V., Goranson, E., Gissen, P., Lilliquist, S. *et al.* (2006) The transmembrane protein meckelin (*MKS3*) is mutated in Meckel–Gruber syndrome and the wpk rat. *Nat. Genet.*, **38**, 191–196.
12. Baala, L., Romano, S., Khaddour, R., Saunier, S., Smith, U.M., Audollent, S., Ozilou, C., Faivre, L., Laurent, N., Foliguet, B. *et al.* (2007) The Meckel–Gruber syndrome Gene, *MKS3*, is mutated in Joubert syndrome. *Am. J. Hum. Genet.*, **80**, 186–194.
13. Brancati, F., Iannicelli, M., Travaglini, L., Mazzotta, A., Bertini, E., Boltshauser, E., D'Arrigo, S., Emma, F., Fazzi, E., Gallizzi, R. *et al.* (2009) MKS3/TMEM67 mutations are a major cause of COACH syndrome, a Joubert syndrome related disorder with liver involvement. *Hum. Mutat.*, **30**, E432–E442.
14. Leitch, C.C., Zaghloul, N.A., Davis, E.E., Stoetzel, C., Diaz-Font, A., Rix, S., Al-Fadhel, M., Lewis, R.A., Eyaid, W., Banin, E. *et al.* (2008)

Hypomorphic mutations in syndromic encephalocele genes are associated with Bardet–Biedl syndrome. *Nat. Genet.*, **40**, 443–448.

15. Dawe, H.R., Smith, U.M., Cullinane, A.R., Gerrelli, D., Cox, P., Badano, J.L., Blair-Reid, S., Sriram, N., Katsanis, N., Attie-Bitach, T. *et al.* (2007) The Meckel–Gruber syndrome proteins MKS1 and meckelin interact and are required for primary cilium formation. *Hum. Mol. Genet.*, **16**, 173–186.

16. Williams, C.L., Winkelbauer, M.E., Schafer, J.C., Michaud, E.J. and Yoder, B.K. (2008) Functional redundancy of the B9 proteins and nephrocystins in *C. elegans* ciliogenesis. *Mol. Biol. Cell*, **19**, 2154–2168.

17. Khaddour, R., Smith, U., Baala, L., Martinovic, J., Clavering, D., Shaffiq, R., Ozilou, C., Cullinane, A., Kyttala, M., Shalev, S. *et al.* (2007) Spectrum of *MKS1* and *MKS3* mutations in Meckel syndrome: a genotype–phenotype correlation. Mutation in brief #960. Online. *Hum. Mutat.*, **28**, 523–524.

18. Clotman, F., Libbrecht, L., Killingsworth, M.C., Loo, C.C., Roskams, T. and Lemaigre, F.P. (2008) Lack of cilia and differentiation defects in the liver of human foetuses with the Meckel syndrome. *Liver Int.*, **28**, 377–384.

19. Gattone, V.H. II, Tourkow, B.A., Trambaugh, C.M., Yu, A.C., Whelan, S., Phillips, C.L., Harris, P.C. and Peterson, R.G. (2004) Development of multiorgan pathology in the *wpk* rat model of polycystic kidney disease. *Anat. Rec.*, **277A**, 384–395.

20. Cook, S.A., Collin, G.B., Bronson, R.T., Naggert, J.K., Liu, D.P., Akeson, E.C. and Davisson, M.T. (2009) A mouse model for Meckel syndrome type 3. *J. Am. Soc. Nephrol.*, **20**, 753–764.

21. Ross, A.J., May-Simera, H., Eichers, E.R., Kai, M., Hill, J., Jagger, D.J., Leitch, C.C., Chapple, J.P., Munro, P.M., Fisher, S. *et al.* (2005) Disruption of Bardet–Biedl syndrome ciliary proteins perturbs planar cell polarity in vertebrates. *Nat. Genet.*, **37**, 1135–1140.

22. Ferrante, M.I., Zullo, A., Barra, A., Bimonte, S., Messaddeq, N., Studer, M., Dolle, P. and Franco, B. (2006) Oral-facial-digital type I protein is required for primary cilia formation and left-right axis specification. *Nat. Genet.*, **38**, 112–117.

23. Smith, L.A., Bukanov, N.O., Husson, H., Russo, R.J., Barry, T.C., Taylor, A.L., Beier, D.R. and Ibraghimov-Beskrovnaya, O. (2006) Development of polycystic kidney disease in juvenile cystic kidney mice: insights into pathogenesis, ciliary abnormalities, and common features with human disease. *J. Am. Soc. Nephrol.*, **17**, 2821–2831.

24. Masyuk, T.V., Huang, B.Q., Ward, C.J., Masyuk, A.I., Yuan, D., Splinter, P.L., Punyashthiti, R., Ritman, E.L., Torres, V.E., Harris, P.C. *et al.* (2003) Defects in cholangiocyte fibrocystin expression and ciliary structure in the PCK rat. *Gastroenterology*, **125**, 1303–1310.

25. Woollard, J.R., Punyashtiti, R., Richardson, S., Masyuk, T.V., Whelan, S., Huang, B.Q., Lager, D.J., vanDeursen, J., Torres, V.E., Gattone, V.H. *et al.* (2007) A mouse model of autosomal recessive polycystic kidney disease with biliary duct and proximal tubule dilatation. *Kidney Int.*, **72**, 328–336.

26. Nishimura, D.Y., Fath, M., Mullins, R.F., Searby, C., Andrews, M., Davis, R., Andorf, J.L., Mykytyn, K., Swiderski, R.E., Yang, B. *et al.* (2004) *Bbs2*-null mice have neurosensory deficits, a defect in social dominance, and retinopathy associated with mislocalization of rhodopsin. *Proc. Natl Acad. Sci. USA*, **101**, 16588–16593.

27. Davis, R.E., Swiderski, R.E., Rahmouni, K., Nishimura, D.Y., Mullins, R.F., Agassandian, K., Philp, A.R., Searby, C.C., Andrews, M.P., Thompson, S. *et al.* (2007) A knockin mouse model of the Bardet–Biedl syndrome 1 M390R mutation has cilia defects, ventriculomegaly, retinopathy, and obesity. *Proc. Natl Acad. Sci. USA*, **104**, 19422–19427.

28. Mykytyn, K., Mullins, R.F., Andrews, M., Chiang, A.P., Swiderski, R.E., Yang, B., Braun, T., Casavant, T., Stone, E.M. and Sheffield, V.C. (2004) Bardet–Biedl syndrome type 4 (BBS4)-null mice implicate Bbs4 in flagella formation but not global cilia assembly. *Proc. Natl Acad. Sci. USA*, **101**, 8664–8669.

29. Fath, M.A., Mullins, R.F., Searby, C., Nishimura, D.Y., Wei, J., Rahmouni, K., Davis, R.E., Tayeh, M.K., Andrews, M., Yang, B. *et al.* (2005) Mks-null mice have a phenotype resembling Bardet–Biedl syndrome. *Hum. Mol. Genet.*, **14**, 1109–1118.

30. Pazour, G.J., Baker, S.A., Deane, J.A., Cole, D.G., Dickert, B.L., Rosenbaum, J.L., Witman, G.B. and Besharse, J.C. (2002) The intraflagellar transport protein, IFT88, is essential for vertebrate photoreceptor assembly and maintenance. *J. Cell Biol.*, **157**, 103–113.

31. den Hollander, A.I., Koenekoop, R.K., Yzer, S., Lopez, I., Arends, M.L., Voesenek, K.E., Zonneveld, M.N., Strom, T.M., Meitinger, T., Brunner,

32. Noor, A., Windpassinger, C., Patel, M., Stachowiak, B., Mikhailov, A., Azam, M., Irfan, M., Siddiqui, Z.K., Naeem, F., Paterson, A.D. *et al.* (2008) CC2D2A, encoding a coiled-coil and C2 domain protein, causes autosomal-recessive mental retardation with retinitis pigmentosa. *Am. J. Hum. Genet.*, **82**, 1011–1018.

33. Nauli, S.M., Alenghat, F.J., Luo, Y., Williams, E., Vassilev, P., Li, X., Elia, A.E., Lu, W., Brown, E.M., Quinn, S.J. *et al.* (2003) Polycystins 1 and 2 mediate mechanosensation in the primary cilium of kidney cells. *Nat. Genet.*, **33**, 129–137.

34. Xu, C., Rossetti, S., Jiang, L., Harris, P.C., Brown-Glaberman, U., Wandinger-Ness, A., Bacallao, R. and Alper, S.L. (2007) Human ADPKD primary cyst epithelial cells with a novel, single codon deletion in the *PKD1* gene exhibit defective ciliary polycystin localization and loss of flow-induced Ca2+ signaling. *Am. J. Physiol. Renal Physiol.*, **292**, F930–F945.

35. Shiba, D., Takamatsu, T. and Yokoyama, T. (2005) Primary cilia of inv/inv mouse renal epithelial cells sense physiological fluid flow: bending of primary cilia and Ca2+ influx. *Cell Struct. Funct.*, **30**, 93–100.

36. Lin, F., Hiesberger, T., Cordes, K., Sinclair, A.M., Goldstein, L.S., Somlo, S. and Igarashi, P. (2003) Kidney-specific inactivation of the KIF3A subunit of kinesin-II inhibits renal ciliogenesis and produces polycystic kidney disease. *Proc. Natl Acad. Sci. USA*, **100**, 5286–5291.

37. Pazour, G.J., Dickert, B.L., Vucica, Y., Seeley, E.S., Rosenbaum, J.L., Witman, G.B. and Cole, D.G. (2000) *Chlamydomonas IFT*88 and its mouse homologue, polycystic kidney disease gene *Tg*737, are required for assembly of cilia and flagella. *J. Cell Biol.*, **151**, 709–718.

38. Bergmann, C., Fliegauf, M., Bruchle, N.O., Frank, V., Olbrich, H., Kirschner, J., Schermer, B., Schmedding, I., Kispert, A., Kranzlin, B. *et al.* (2008) Loss of nephrocystin-3 function can cause embryonic lethality, Meckel–Gruber-like syndrome, *situs inversus*, and renal-hepatic-pancreatic dysplasia. *Am. J. Hum. Genet.*, **82**, 959–970.

39. Muchatuta, M.N., Gattone, V.H. II, Witzmann, F.A. and Blazer-Yost, B.L. (2009) Structural and functional analyses of liver cysts from the BALB/c-cpk mouse model of polycystic kidney disease. *Exp. Biol. Med. (Maywood)*, **234**, 17–27.

40. Tam, L.W., Dentler, W.L. and Lefebvre, P.A. (2003) Defective flagellar assembly and length regulation in *LF3* null mutants in *Chlamydomonas*. *J. Cell Biol.*, **163**, 597–607.

41. Wemmer, K.A. and Marshall, W.F. (2007) Flagellar length control in *Chlamydomonas*—a paradigm for organelle size regulation. *Int. Rev. Cytol.*, **260**, 175–212.

42. Marshall, W.F., Qin, H., Rodrigo Brenni, M. and Rosenbaum, J.L. (2005) Flagellar length control system: testing a simple model based on intraflagellar transport and turnover. *Mol. Biol. Cell*, **16**, 270–278.

43. Marshall, W.F. and Rosenbaum, J.L. (2001) Intraflagellar transport balances continuous turnover of outer doublet microtubules: implications for flagellar length control. *J. Cell Biol.*, **155**, 405–414.

44. Yoder, B.K., Tousson, A., Millican, L., Wu, J.H., Bugg, C.E. Jr, Schafer, J.A. and Balkovetz, D.F. (2002) Polaris, a protein disrupted in orpk mutant mice, is required for assembly of renal cilium. *Am. J. Physiol. Renal Physiol.*, **282**, F541–F552.

45. Brown, N.E. and Murcia, N.S. (2003) Delayed cystogenesis and increased ciliogenesis associated with the re-expression of polaris in *Tg737* mutant mice. *Kidney Int.*, **63**, 1220–1229.

46. D'Assoro, A.B., Lingle, W.L. and Salisbury, J.L. (2002) Centrosome amplification and the development of cancer. *Oncogene*, **21**, 6146–6153.

47. Fukasawa, K. (2005) Centrosome amplification, chromosome instability and cancer development. *Cancer Lett.*, **230**, 6–19.

48. Fukasawa, K. (2007) Oncogenes and tumour suppressors take on centrosomes. *Nat. Rev. Cancer*, **7**, 911–924.

49. Battini, L., Macip, S., Fedorova, E., Dikman, S., Somlo, S., Montagna, C. and Gusella, G.L. (2008) Loss of polycystin-1 causes centrosome amplification and genomic instability. *Hum. Mol. Genet.*, **17**, 2819–2833.

50. Gogusev, J., Murakami, I., Doussau, M., Telvi, L., Stojkoski, A., Lesavre, P. and Droz, D. (2003) Molecular cytogenetic aberrations in autosomal dominant polycystic kidney disease tissue. *J. Am. Soc. Nephrol.*, **14**, 359–366.

51. Burtey, S., Riera, M., Emilie, R., Pennenkamp, P., Rance, R., Luciani, J., Dworniczak, B., Mattei, M.G. and Fontes, M. (2008) Centrosome overduplication and mitotic instability in PKD2 transgenic lines. *Cell Biol. Int.*, **74**, 1193–1198.

H.G. *et al.* (2006) Mutations in the *CEP290* (NPHP6) gene are a frequent cause of Leber congenital amaurosis. *Am. J. Hum. Genet.*, **79**, 556–561.

52. Duffy, J.L. and Suzuki, Y. (1968) Ciliated human renal proximal tubular cells. Observations in three cases of hypercalcemia. *Am. J. Pathol.*, **53**, 609–616.
53. Hassan, M.O. and Subramanyan, S. (1995) Ciliated renal tubular cells in crescentic glomerulonephritis. *Ultrastruct. Pathol.*, **19**, 201–203.
54. Katz, S.M. and Morgan, J.J. (1984) Cilia in the human kidney. *Ultrastruct. Pathol.*, **6**, 285–294.
55. Lungarella, G., de Santi, M.M. and Tosi, P. (1984) Ultrastructural study of the ciliated cells from renal tubular epithelium in acute progressive glomerulonephritis. *Ultrastruct. Pathol.*, **6**, 1–7.
56. Ong, A.C. and Wagner, B. (2005) Detection of proximal tubular motile cilia in a patient with renal sarcoidosis associated with hypercalcemia. *Am. J. Kidney Dis.*, **45**, 1096–1099.
57. Liu, Y., Pathak, N., Kramer-Zucker, A. and Drummond, I.A. (2007) Notch signaling controls the differentiation of transporting epithelia and multiciliated cells in the zebrafish pronephros. *Development*, **134**, 1111–1122.
58. Kramer-Zucker, A.G., Olale, F., Haycraft, C.J., Yoder, B.K., Schier, A.F. and Drummond, I.A. (2005) Cilia-driven fluid flow in the zebrafish pronephros, brain and Kupffer's vesicle is required for normal organogenesis. *Development*, **132**, 1907–1921.
59. Peel, N., Stevens, N.R., Basto, R. and Raff, J.W. (2007) Overexpressing centriole-replication proteins *in vivo* induces centriole overduplication and *de novo* formation. *Curr. Biol.*, **17**, 834–843.
60. Rodrigues-Martins, A., Riparbelli, M., Callaini, G., Glover, D.M. and Bettencourt-Dias, M. (2007) Revisiting the role of the mother centriole in centriole biogenesis. *Science*, **316**, 1046–1050.
61. Fischer, E., Legue, E., Doyen, A., Nato, F., Nicolas, J.F., Torres, V., Yaniv, M. and Pontoglio, M. (2006) Defective planar cell polarity in polycystic kidney disease. *Nat. Genet.*, **38**, 21–23.
62. Katsanis, N. (2006) Ciliary proteins and exencephaly. *Nat. Genet.*, **38**, 135–136.
63. Simons, M., Gloy, J., Ganner, A., Bullerkotte, A., Bashkurov, M., Kronig, C., Schermer, B., Benzing, T., Cabello, O.A., Jenny, A. *et al.* (2005) Inversin, the gene product mutated in nephronophthisis type II, functions as a molecular switch between Wnt signaling pathways. *Nat. Genet.*, **37**, 537–543.
64. Park, T.J., Haigo, S.L. and Wallingford, J.B. (2006) Ciliogenesis defects in embryos lacking inturned or fuzzy function are associated with failure of planar cell polarity and Hedgehog signaling. *Nat. Genet.*, **38**, 303–311.
65. Torban, E., Kor, C. and Gros, P. (2004) Van Gogh-like2 (Strabismus) and its role in planar cell polarity and convergent extension in vertebrates. *Trends Genet.*, **20**, 570–577.